iScience

CellPress
OPEN ACCESS

Article

Prenatal hormone stress triggers embryonic cardiac hypertrophy outcome by ubiquitin-dependent degradation of mitochondrial mitofusin 2

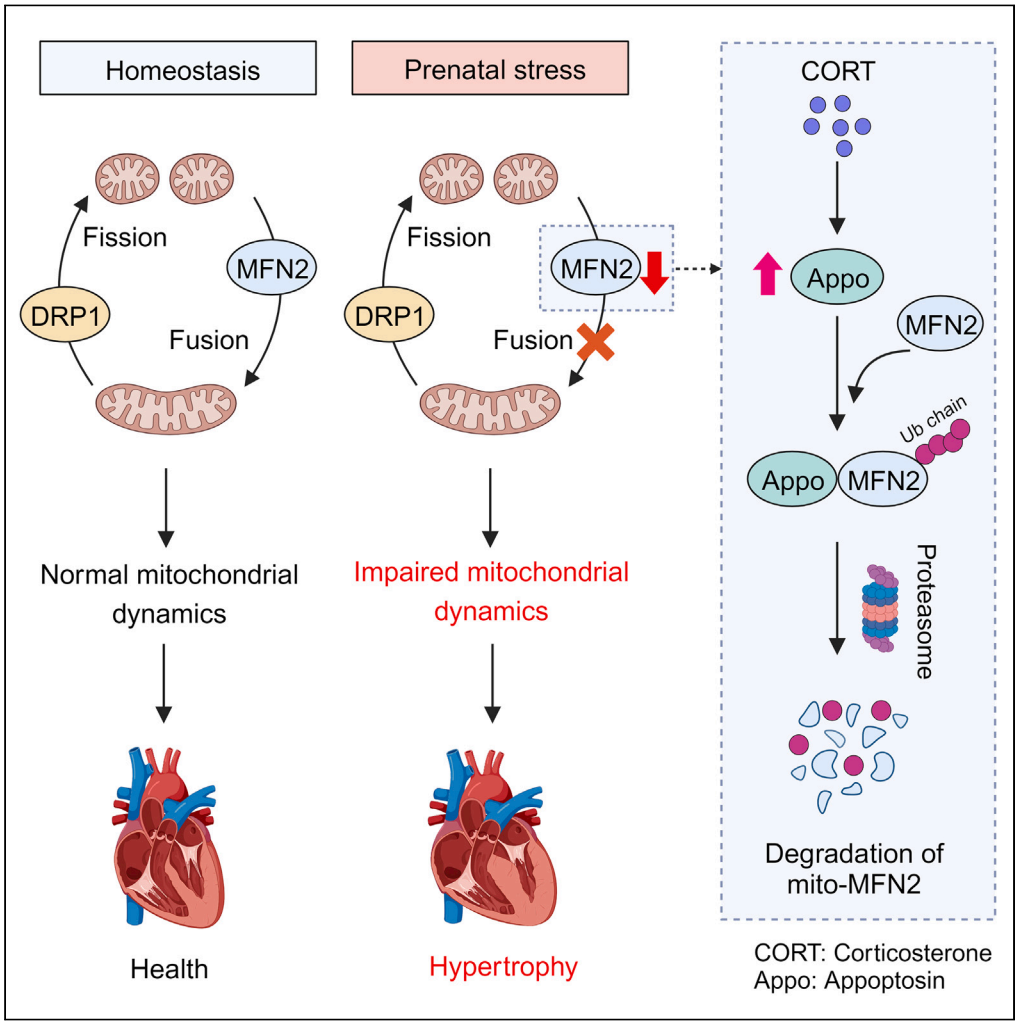

Chang-Yu Yan, Yue Ye, Han-Lu Mu, ..., Hiroshi Kurihara, Yi-Fang Li, Rong-Rong He

liyifang706@jnu.edu.cn (Y.-F.L.)
rongronghe@jnu.edu.cn (R.-R.H.)

Highlights

CORT contributes to the cardiac hypertrophy of offsprings exposed to prenatal stress

CORT causes abnormal mitochondrial fusion and dysfunction of energy metabolism

CORT reduces the level of mitochondrial MFN2

Appoptosin is induced by CORT to trigger ubiquitination degradation of MFN2

Yan et al., iScience 27, 108690
January 19, 2024
https://doi.org/10.1016/j.isci.2023.108690

iScience

CellPress
OPEN ACCESS

Article

Prenatal hormone stress triggers embryonic cardiac hypertrophy outcome by ubiquitin-dependent degradation of mitochondrial mitofusin 2

Chang-Yu Yan,[1,5] Yue Ye,[1,5] Han-Lu Mu,[1] Tong Wu,[1] Wen-Shan Huang,[1] Yan-Ping Wu,[1] Wan-Yang Sun,[1] Lei Liang,[1] Wen-Jun Duan,[1] Shu-Hua Ouyang,[1] Rui-Ting Huang,[2] Rong Wang,[3] Xin-Xin Sun,[4] Hiroshi Kurihara,[1] Yi-Fang Li,[1,*] and Rong-Rong He[1,2,3,6,*]

SUMMARY

Prenatal stress has been extensively documented as a contributing factor to adverse cardiac development and function in fetuses and infants. The release of glucocorticoids (GCs), identified as a significant stressor, may be a potential factor inducing cardiac hypertrophy. However, the underlying mechanism remains largely unknown. Herein, we discovered that corticosterone (CORT) overload induced cardiac hypertrophy in embryonic chicks and fetal mice *in vivo*, as well as enlarged cardiomyocytes *in vitro*. The impaired mitochondria dynamics were observed in CORT-exposed cardiomyocytes, accompanied by dysfunction in oxidative phosphorylation and ATP production. This phenomenon was found to be linked to decreased mitochondrial fusion protein mitofusin 2 (MFN2). Subsequently, we found that CORT facilitated the ubiquitin-proteasome-system-dependent degradation of MFN2 with an enhanced binding of appoptosin to MFN2, serving as the underlying cause. Collectively, our findings provide a comprehensive understanding of the mechanisms by which exposure to stress hormones induces cardiac hypertrophy in fetuses.

INTRODUCTION

Cardiac hypertrophy is a type of adaptive and compensatory response to pressure and volume overload caused by various stimuli.[1] Initially, cardiac hypertrophy confers a beneficial effect, as it supports the cardiac pump function and reduces wall pressure to match the increased workload. However, prolonged exposure to such stimuli can lead to pathological hypertrophy and irreversible cardiac dysfunction, eventually culminating in heart failure with high morbidity and mortality.[2,3] Mechanistically, cardiac hypertrophy is orchestrated by diverse cellular signaling pathways, upregulation of pro-hypertrophic genes, mitochondrial dysfunction, and metabolic reprogramming.[4,5]

Prenatal stress, like psychological stress, is considered to produce a sub-optional environment for embryo, which can have deleterious effects on fetal cardiovascular development, such as the emergence of cardiac hypertrophy.[6–8] In fact, emotional stress has long been recognized in traditional Chinese medicine as a crucial mechanism leading to disease susceptibility.[9] The primary response of the organism to stress is the hyperactivation of the hypothalamus-pituitary-adrenal (HPA) and hypothalamus-pituitary-thyroid (HPT) axes, resulting in abnormal release of glucocorticoids (GCs) and thyroid hormone. Among these stressors, the activation of the HPA axis, which induces the production of cortisol/corticosterone (CORT), the primary GCs in humans/rodents, has been widely reported to be associated with the adverse development of embryos. Importantly, abnormal cortisol levels in the mother can result in elevated cortisol levels in the fetus.[10] Several clinical studies have shown that exposure to synthetic GCs during pregnancy can lead to myocardial remodeling and hypertrophy in infants.[11–13] Some animal studies also have indicated that dexamethasone treatment for neonatal infants can contribute to cardiac hypertrophy.[14,15] In addition, cardiac steroidogenesis was activated with an increase in cardiac GCs level in hypertrophied mice hearts.[16] However, the underlying molecular mechanisms of stress-hormone-GCs-related cardiac hypertrophy remain incompletely understood, posing challenges for drug discovery and development.[17]

Mitochondrial dysfunction is widely recognized as a key contributor to cardiac hypertrophy and subsequent heart failure, involving mitochondrial biosynthesis, morphology, energy status, redox balance, and Ca^{2+} homeostasis.[18–21] Additionally, the mitochondrial dynamic

[1]Guangdong Engineering Research Center of Chinese Medicine & Disease Susceptibility, International Cooperative Laboratory of Traditional Chinese Medicine Modernization and Innovative Drug Development of Chinese Ministry of Education (MOE), Guangdong Province Key Laboratory of Pharmacodynamic Constituents of TCM and New Drugs Research, Jinan University, Guangzhou 510632, China
[2]State Key Laboratory of Quality Research in Chinese Medicine, Macau University of Science and Technology, Macau 999078, China
[3]School of Chinese Materia Medica and Yunnan Key Laboratory of Southern Medicinal Utilization, Yunnan University of Chinese Medicine, Kunming 650500, China
[4]Jiujiang Maternal and Child Health Hospital, Jiujiang 332000, China
[5]These authors contributed equally
[6]Lead contact
*Correspondence: liyifang706@jnu.edu.cn (Y.-F.L.), rongronghe@jnu.edu.cn (R.-R.H.)
https://doi.org/10.1016/j.isci.2023.108690

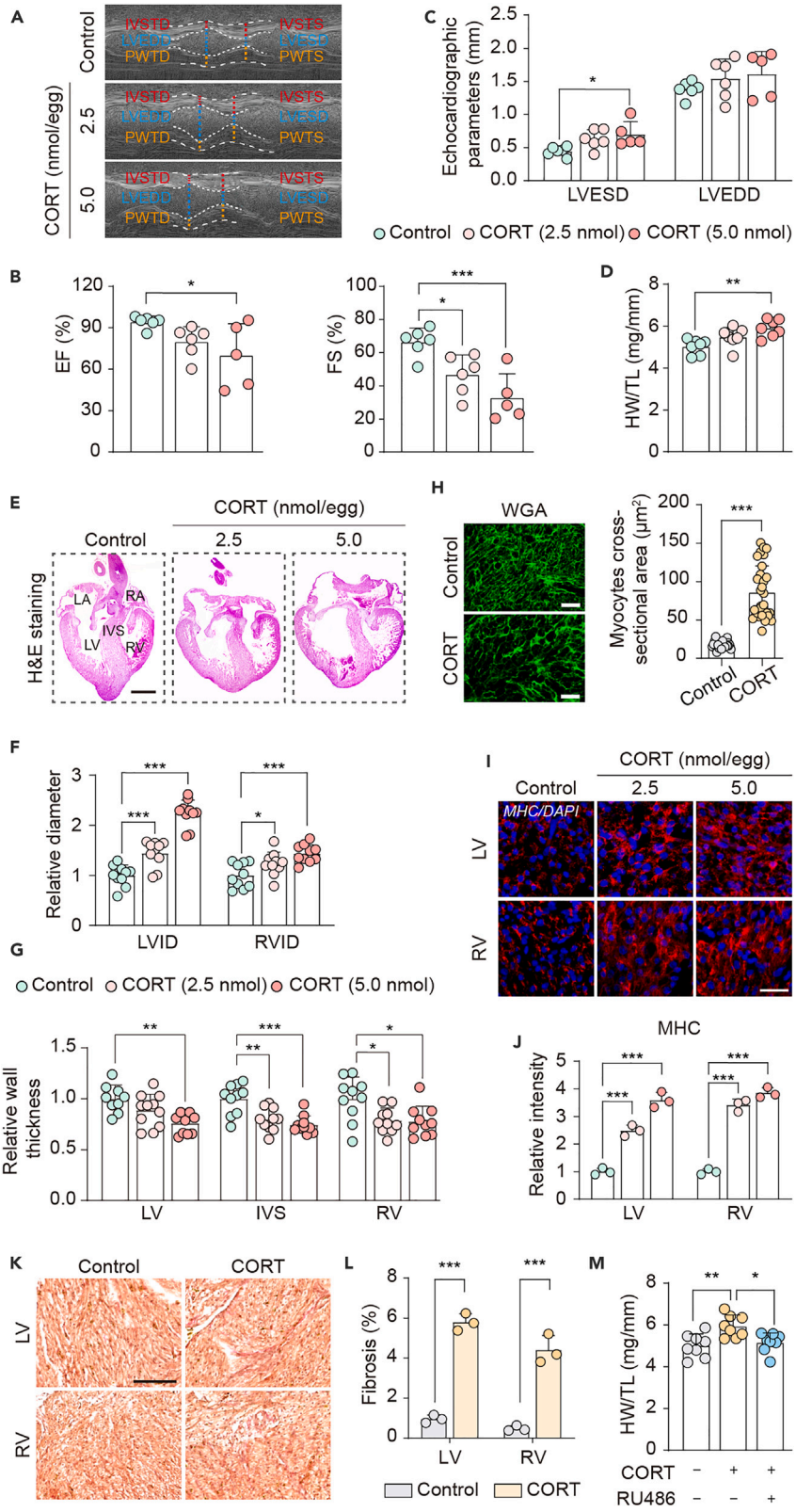
A
Control
2.5
5.0
CORT (nmol/egg)
IVSTD
LVEDD
PWTD
IVSTS
LVESD
PWTS
C
Echocardiographic parameters (mm)
LVESD
LVEDD
Control
CORT (2.5 nmol)
CORT (5.0 nmol)
B
EF (%)
FS (%)
D
HW/TL (mg/mm)
E
CORT (nmol/egg)
Control
2.5
5.0
H&E staining
LA
RA
IVS
LV
RV
H
WGA
Control
CORT
Myocytes cross-sectional area (μm²)
F
Relative diameter
LVID
RVID
G
Relative wall thickness
LV
IVS
RV
I
CORT (nmol/egg)
Control
2.5
5.0
MHC/DAPI
LV
RV
J
MHC
Relative intensity
K
Control
CORT
LV
RV
L
Fibrosis (%)
Control
CORT
M
HW/TL (mg/mm)
CORT
RU486

Figure 1. Cardiac hypertrophy is induced in developing chicken embryos upon exposure to CORT

(A) M-mode echocardiography for chicken embryos on the EDD 14. LVEDD, left ventricular end-diastolic dimension; LVESD, left ventricular end-systolic dimension; IVSTD, interventricular septal thickness in diastole; IVSTS, interventricular septal thickness in systole; PWTD, posterior wall thickness in diastole; PWTS, posterior wall thickness in systole (n = 5–6).

(B and C) Cardiac function parameters ejection fraction (EF), fractional shortening (FS), LVEDD, and LVESD in (A).

(D) The ratio of heart weight (HW) to tibial length (TL) of EDD14 chicken embryos (n = 7).

(E) H&E staining of the whole heart of EDD14 chicken embryos. Scale bar: 2 mm. (n = 10). LA, left atrium; LV, left ventricle; RA, right atrium; RV, right ventricle; IVS, interventricular septum.

(F and G) Left ventricular internal diameter (LVID) and right ventricular internal diameter (RVID); relative wall thickness of LV, IVS, and RV in (E).

(H) WGA staining of hearts of chicken embryos and myocytes cross-sectional area. Scale bar: 25 μm. (n = 3).

(I and J) Immunofluorescence detection of MHC and quantitative analysis of MHC level by ImageJ. Scale bar: 20 μm. (n = 3).

(K and L) Sirius Red staining of the hearts of EDD14 chicken embryos treated with CORT (5.0 nmol/egg) and the quantitative analysis of collagen fibers. Scale bar: 100 μm. (n = 3).

(M) The ratio of HW to TL in CORT (5.0 nmol)-treated EDD14 chicken embryos with or without RU486 (5.0 nmol) (n = 8). Data are expressed as the mean ± SD and subjected to statistical analysis using unpaired Student's t test or one-way ANOVA followed by Dunnett's multiple comparison test, *$p < 0.05$, **$p < 0.01$, ***$p < 0.001$ vs. the indicated group.

process of fusion and fission is closely linked to mitochondrial function, and mitochondrial fragmentation due to unbalanced dynamics is an important factor in cardiac hypertrophy.[22–24] Significantly, improving the structure and function of mitochondria has become an essential approach for the treatment of cardiac hypertrophy.[25–27] The dynamics of mitochondria are regulated by some mitochondria-shaping proteins, such as fission protein dynamin-related protein 1 (Drp1), mitochondrial fission factor (MFF), and fusion proteins OPA1 and mitofusin1/2 (MFN1/2). Numerous studies have demonstrated that interventions targeting these proteins can modulate mitochondrial dynamics and affect the process of cardiac hypertrophy.[28–33] In the current study, we unravel that prenatal stress hormone CORT could induce fragmentation and dysfunction of mitochondria, resulting in cardiac hypertrophy in developing chicken and mice embryos. Mechanically, this stress hormone promotes proteasomal degradation of mitochondrial MFN2 by enhancing interaction between MFN2 and appoptosin.

RESULTS

Cardiac hypertrophy is induced in developing chicken embryos upon exposure to CORT

We first investigated the impact of CORT exposure during pregnancy on the hearts of chicken embryos, a widely well-established model for studying embryonic development (Figure S1A). Administration of exogenous CORT resulted in elevated plasma CORT levels, indicating successful delivery of the hormone to the embryos (Figure S1B). To evaluate the consequences of CORT treatment, we employed echocardiography to assess cardiac function in embryonic development day 14 (EDD14) chicken embryo (Figure 1A). Notably, CORT treatment led to impaired cardiac function, as demonstrated by a significant reduction in both ejection fraction (EF) and fractional shortening (FS) (Figure 1B), accompanied by an increase in left ventricular end-systolic dimension (LVESD) (Figure 1C). Additionally, CORT-exposed embryos displayed an elevated heart weight (HW) to tibial length (TL) ratio, an indicator of cardiac dysfunction (Figure 1D). We further characterized the changes in the hearts of embryos through histopathological examination, which revealed a hypertrophic response in the hearts of CORT-treated embryos (Figure 1E). Notably, the hypertrophic hearts exhibited eccentric hypertrophy, characterized by a substantial increase in both left ventricular and right ventricular internal diameter (LVID and RVID), coupled with a reduction in wall thickness of left ventricle, right ventricle, and interventricular septum (Figures 1F and 1G). Besides, the application of FITC-labeled WGA enabled visualization of cardiomyocyte outlines. As exhibited in Figure 1H, cardiomyocytes size of left ventricle was evidently increased in CORT group. In addition, we conducted immunofluorescence staining to assess the expression of myosin heavy chain (MHC), a marker of myocardial hypertrophy. CORT treatment resulted in increased MHC expression in both the left ventricle and right ventricle (Figures 1I and 1J). Myocardial fibroblasts are activated to synthesize collagen, and excess deposition of collagen can lead to pathological fibrosis, which is an important characteristic feature of cardiac hypertrophy.[34] In the subsequent analysis, we assessed the abundance of collagen fibers within myocardial tissue using Sirius Red staining and observed a significant fibrosis induced by CORT according to the quantification of the fibrotic area (Figures 1K and 1L). Furthermore, the actions of CORT are typically mediated through its binding to the glucocorticoid receptor (GR), a member of the nuclear receptor superfamily of transcription factors. As illustrated in Figures 1M and S1C, RU486, a specific GR antagonist, effectively suppressed the CORT-induced cardiac hypertrophy pathology and the elevated ratio of HW to TL. This observation indicates that CORT triggers cardiac remodeling in a GR-dependent manner. The findings aforementioned strongly suggest that CORT induces cardiac hypertrophy in developing chicken embryos.

Maternal mice exposed to CORT during pregnancy results in cardiomegaly in offspring

Subsequently, we aimed to elucidate the hypertrophic effects of prenatal exposure to CORT on embryonic hearts in mammalian models by the administration of exogenous CORT to pregnant mice (Figure S2). Our findings revealed that neonatal mice exhibited cardiac dysfunction as evidenced by echocardiography with decreased EF and FS. In addition, this CORT-induced cardiac dysfunction persisted in the offspring at 4 weeks of age (Figures 2A and 2B). Furthermore, we observed a significant increase in LV mass of 4-week-old offspring, despite the absence of significant differences in neonatal mice (Figure 2C). Interestingly, the HW to body weight (BW) ratio were significantly elevated in both neonatal mice and 4-week-old offspring within the CORT treatment group (Figure 2D). Next, we conducted direct observations of pathological changes of the 4-week-old offspring hearts via HE staining, revealing an enlargement of the LV (Figure 2E). As anticipated, cardiomyocytes

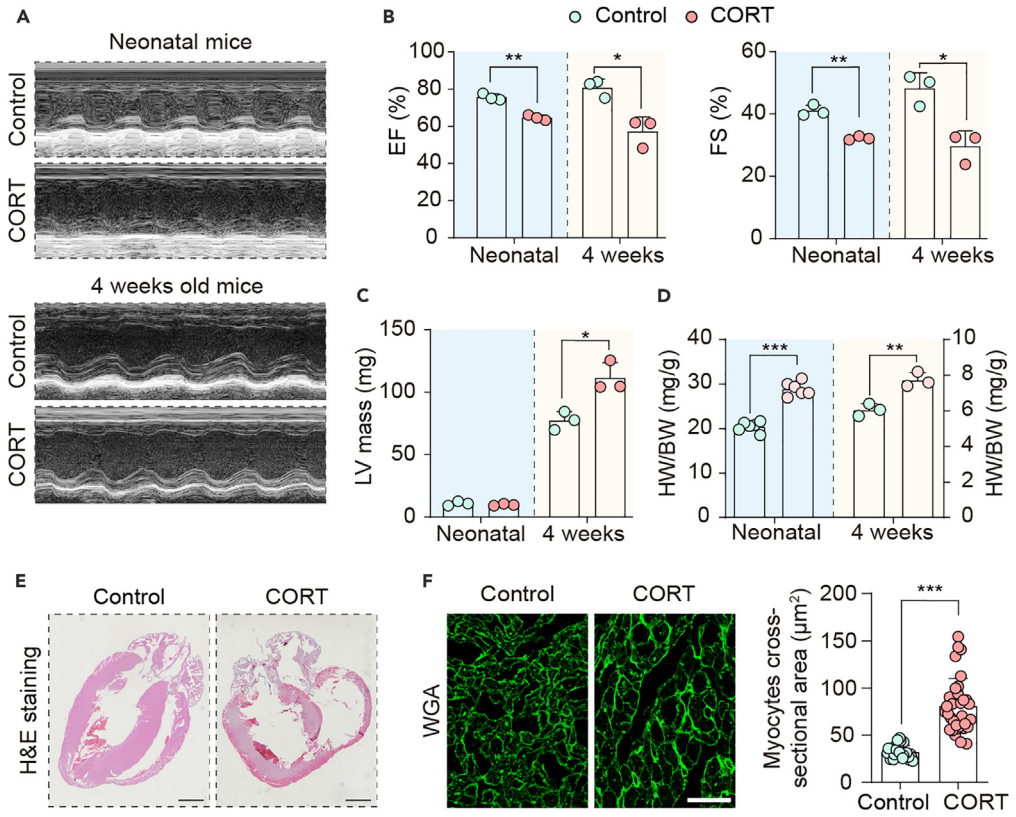

Figure 2. Maternal mice exposed to CORT during pregnancy results in cardiomegaly in offspring

(A) M-mode echocardiography for the neonatal and 4-week-old offspring mice (n = 3).

(B) The cardiac function parameter of echocardiograph in (A), including ejection fraction (EF) and fractional shortening (FS).

(C) LV mass was analyzed in (A).

(D) The ratio of heart weight (HW) to body weight (BW) of the neonatal (n = 3) and 4-week-old (n = 3) mice.

(E) H&E staining of the whole heart of the 4-week-old mice. Scale bar: 1 mm.

(F) WGA staining of cardiomyocyte of the 4-week-old mice. Scale bar: 25 μm. (n = 3). The area of cardiomyocyte was analyzed by ImageJ software. Data are expressed as the mean ± SD and subjected to statistical analysis using unpaired Student's t test, *p < 0.05, **p < 0.01, ***p < 0.001 vs. the indicated group.

in the CORT-treated group exhibited an increased cross-sectional area, as demonstrated by WGA staining, providing further support for the development of cardiomegaly (Figure 2F). Our results demonstrate that prenatal exposure to CORT induces cardiomegaly in offspring mice.

CORT stress provokes cardiomyocyte hypertrophy in H9c2 cells

We proceeded to investigate the role of CORT in cardiomyocyte hypertrophy *in vitro* using H9c2 cell line, a widely utilized cardiomyocyte cell line for the study of cardiac hypertrophy due to its robust hypertrophic responses.[35] To assess alterations in cell size, we employed TRITC-conjugated phalloidin, a probe with a high affinity for filamentous actin (F-actin), enabling visualization of the cell cytoskeleton. Strikingly, the area of H9c2 cell was significantly elevated after CORT (200 μM) treatment, indicating cellular enlargement without observable cytotoxic effects (Figures 3A, 3B, and S3). Furthermore, cell size was quantitatively evaluated by a flow cytometer based on forward scatter (FSC) measurements. Analysis of the FSC-based cell-size distribution revealed a rightward shift in the CORT-treated group, indicative of an increase in cell size. Quantification of the mean FSC signal demonstrated a 1.4-fold increase in cell size following CORT treatment (Figure 3C). Additionally, cardiac hypertrophy is characterized by distinct alterations in gene expression patterns. Therefore, we examined the expression levels of four hypertrophy-related genes, namely *ANP*, *BNP*, *α-SKA*, and *α-MHC*, which exhibited significant up-regulation upon CORT stimulation (Figure 3D). These findings suggest that CORT induces cardiomyocyte hypertrophy *in vitro*.

Impairment of mitochondrial dynamics and disruption of energy metabolism occur as a consequence of CORT exposure

Previous studies have reported that abnormal mitochondrial fission is associated with cardiomyocyte hypertrophy.[36] Therefore, we investigated whether CORT exposure impairs mitochondria dynamics, leading to cardiomegaly. To address this, we examined the morphological changes of mitochondria in the hearts of EDD14 chicken embryos, 4-week-old mice, and H9c2 cells using transmission electron microscopy (TEM). In the control group, myocardial mitochondria in the hearts of chicken embryos appeared tubular and elongated. However, upon

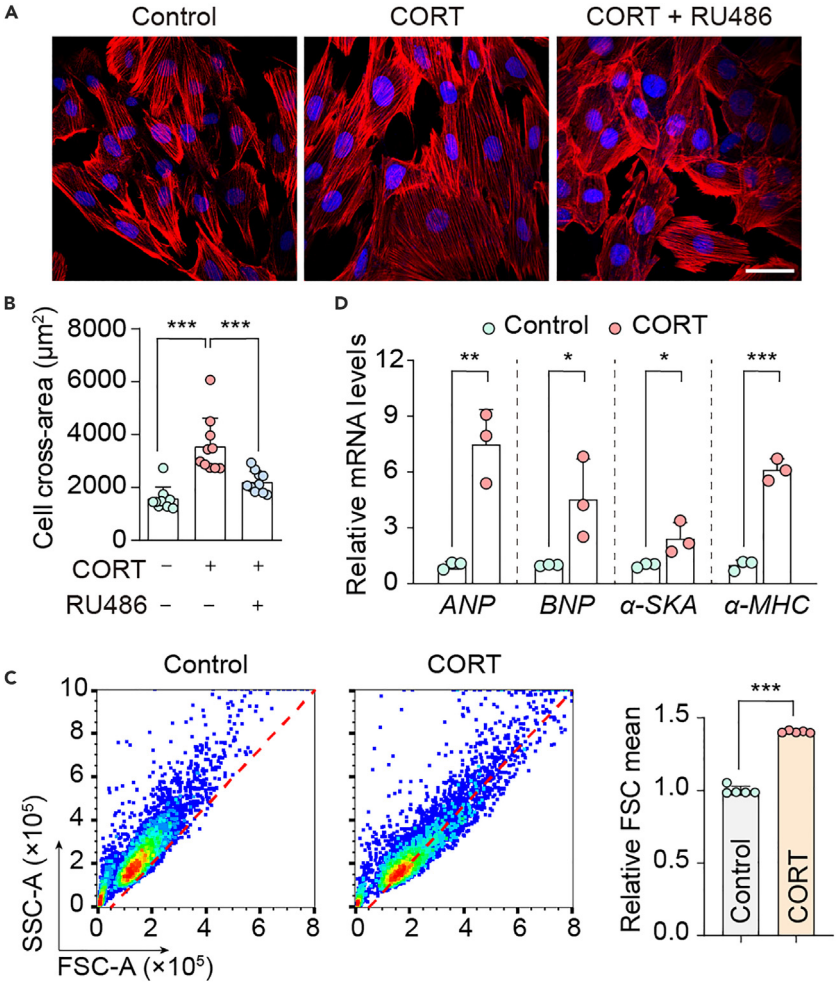

Figure 3. CORT stress provokes cardiomyocyte hypertrophy in H9c2 cells

(A) Representative confocal images of H9c2 cardiomyocyte stained with phalloidin-TRITC. Scale bar: 40 μm.

(B) The cell-cross area of H9c2 cells in (A) was analyzed by ImageJ software.

(C) Flow cytometry detection of H9c2 cells with FSC-A and SSC-A channels and quantitative analysis of mean intensity FSC-A signal (n = 5).

(D) The mRNA levels of four hypertrophy genes, including *ANP*, *BNP*, *α-SKA*, and *α-MHC*, were detected by qPCR (n = 3). Data are expressed as the mean ± SD and subjected to statistical analysis using unpaired Student's t test or one-way ANOVA followed by Dunnett's multiple comparison test, *p < 0.05, **p < 0.01, ***p < 0.001 vs. the indicated group.

CORT stimulation, mitochondria became round and smaller, exhibiting decreased area and aspect ratio. This phenomenon was also observed in the hearts of mice and H9c2 cells (Figure 4A). This intriguing observation prompted us to further assess mitochondrial morphology using the Mito-Red probe and confocal microscopy. As shown in Figure 4B, CORT caused the transformation of long filamentous mitochondria into small puncta-like structures. Of note, this detrimental effect on mitochondria was blocked by RU486, indicating that CORT impaired mitochondria in a GR-dependent manner. Furthermore, CORT treatment significantly decreased mitochondrial membrane potential ($\Delta\psi m$) in H9c2 cells and the hearts of chicken embryos (Figures S4A and S4B).

Given that myocardial contractions heavily rely on mitochondrial energy, we next investigated whether CORT stress affected mitochondrial energy metabolism. Firstly, we assessed the content of ATP in cardiomyocytes and found that CORT resulted in a significant reduction in ATP production in H9c2 cells and the hearts of chicken embryos (Figures 4C and 4D; Figure S4C). Oxidative phosphorylation (OXPHOS) is the primary pathway for ATP synthesis occurring in mitochondria. Therefore, we evaluated the capacity of OXPHOS in H9c2 cells by Seahorse analysis. It was observed that CORT causes a decrease in oxygen consumption rate (OCR) in H9c2 cells, indicating impaired OXPHOS function of mitochondria (Figure 4E). Similarly, we isolated mitochondria from the heart tissue of 4-week-old mice and conducted Seahorse analysis, which also showed a reduction in OCR with CORT treatment (Figure 4F). In addition, the activities of mitochondrial complex enzyme were significantly decreased in H9c2 cells and chicken embryo hearts following CORT treatment (Figures 4G and 4H). The aforementioned results indicate that CORT induces impairment of mitochondrial dynamics and disruption of energy metabolism of cardiomyocyte.

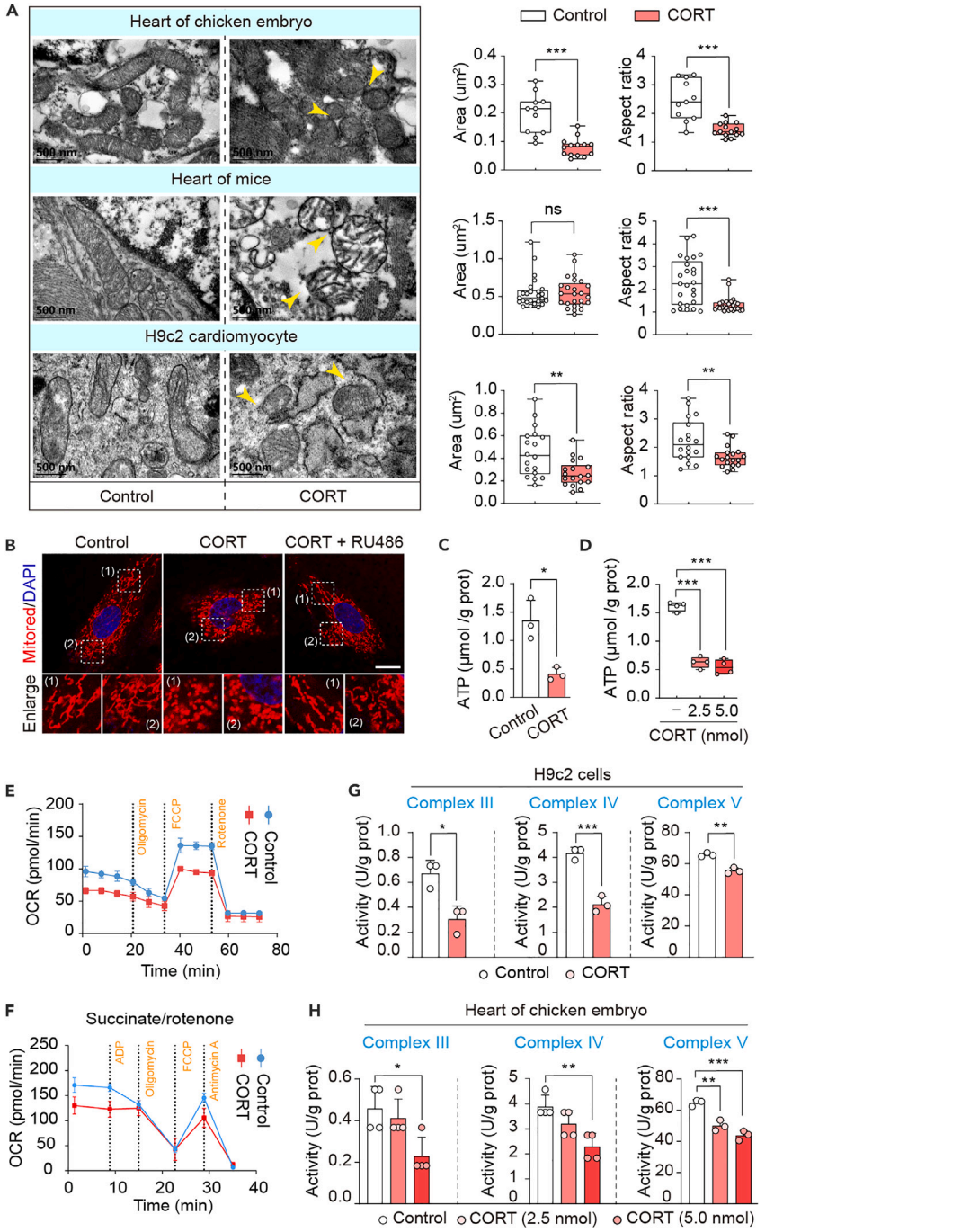

Figure 4. Impairment of mitochondrial dynamics and disruption of energy metabolism occur as a consequence of CORT exposure

(A) Morphology of mitochondria of heart of chicken embryos, heart of 4-week-old mice, and H9c2 cells was detected by transmission electron microscopy (TEM). Scale bar: 500 nm. The yellow arrows represent impaired mitochondria. The quantitative analysis of area and aspect ratio of mitochondria was performed by ImageJ software. Center line, median; box, interquartile range; whiskers, range; bars, maximum and minimum.

(B) The mitochondria of H9c2 cells were labeled with Mito-Red probe and examined by confocal microscopy. Scale bar: 10 μm.

(C and D) The content of ATP in H9c2 cells (n = 3) or heart of chicken embryos (n = 4). In (D), center line, median; box, interquartile range; whiskers, range; bars, maximum and minimum.

(E) Seahorse analysis of OXPHOS in H9c2 cells (n = 4).

Figure 4. *Continued*

(F) Seahorse analysis of OXPHOS of separated heart mitochondria in 4-week-old mice (n = 5).

(G and H) Activities of mitochondrial respiratory chain complex in H9c2 cells (n = 3) or hearts of EDD14 chicken embryo were measured by commercial kits (n = 3–4). Data are expressed as the mean ± SD (unless otherwise indicated) and subjected to statistical analysis using unpaired Student's t test or one-way ANOVA followed by Dunnett's multiple comparison test; ns (not significant); *p < 0.05, **p < 0.01, ***p < 0.001 vs. the indicated group.

The reduction in mitochondrial MFN2 protein contributes to CORT-induced mitochondrial dysfunction and cardiomyocyte hypertrophy

Based on the aforementioned findings indicating that CORT impairs the dynamic processes of cardiomyocyte mitochondria, we next sought to elucidate the underlying molecular mechanism. The dynamic regulation of mitochondria is governed by some mitochondria-shaping proteins, such as the fusion protein MFN2 and the fission protein Drp-1. Initially, we observed that CORT increased the levels of MFN2 while having no effects on Drp1 and its phosphorylation in H9c2 cells (Figure S5). Considering the subcellular localization of MFN2, we isolated mitochondria to evaluate its expression within these organelles, directly influencing mitochondrial dynamics. Intriguingly, CORT decreased the presence of MFN2 within H9c2 cell mitochondria (Figure 5A). We further observed a similar trend in the hearts of chicken embryos, where CORT reduced MFN2 expression in mitochondria but increased it within the endoplasmic reticulum (ER) (Figure 5B). Moreover, a significant loss of MFN2 protein in mitochondria was also detected in the hearts of offspring mice upon maternal exposure to CORT (Figure 5C). Therefore, these findings led us to propose that the deficiency of MFN2 in mitochondria may contribute to impaired fusion dynamics and cardiac hypertrophy. To validate this hypothesis, we conducted overexpression of MFN2 in CORT-treated H9c2 cells and confirmed that supplementation of MFN2 alleviated CORT-induced cardiomyocyte enlargement (Figure 5D) and restored the compromised mitochondrial network (Figure 5E). Taken together, these results suggest that CORT selectively reduces the presence of MFN2 in mitochondria, which is associated with CORT-induced mitochondrial dysfunction and cardiomyocyte enlargement.

CORT triggers proteasome-dependent degradation of mitochondrial MFN2

Next, we explored how CORT reduced the content of MFN2 in mitochondria. To begin, we employed cycloheximide (CHX), a well-known inhibitor of eukaryotic translation, to block protein synthesis and examine whether CORT influences the degradation of mitochondrial MFN2. The results revealed that CORT promoted degradation of MFN2 in mitochondria, leading to a reduction in its half-life from 4.8 h to 1.0 h (Figure 6A). Intracellular protein degradation pathways primarily involve the ubiquitin-proteasome system (UPS) and autophagy pathway. To gain deeper insights into the mechanism of mitochondrial MFN2 degradation, we separately utilized the proteasome inhibitor MG-132 and the autophagy inhibitor 3-MA to assess their effects on CORT-induced MFN2 degradation. Notably, MG-132 restored the level of mitochondrial MFN2, whereas 3-MA showed no such effect (Figures 6B and 6C). Thus, proteasomal degradation of MFN2 in mitochondria appears to be a pivotal factor contributing to its decreased protein level under CORT treatment. Subsequently, we performed co-immunoprecipitation experiments in H9c2 cells to verify the ubiquitination modification of mitochondrial MFN2. As depicted in Figure 6D, mitochondrial MFN2 ubiquitination was induced by CORT, which was inhibited by RU486. This implies that the degradation of mitochondrial MFN2 by CORT is also dependent on the GR. Additionally, the combination of MG-132 further augmented ubiquitination of mitochondrial MFN2 (Figure 6E). Furthermore, CORT-induced ubiquitination of MFN2 was also observed in heart tissues of chicken embryos and offspring mice (Figures 6F and 6G). The seven lysine residues (K6, K11, K27, K29, K33, K48, and K63) of ubiquitin protein can be employed to form various types of poly-ubiquitin linkage, which are associated with different cellular functions and molecular events. Normally, K48-linked polyubiquitin chains are involved in proteasomal degradation of substrate proteins, whereas K63-linked polyubiquitin modification regulates proteasome-independent functions such as signal transduction, protein-protein interactions, control of activity, or conformational changes.[37] Hence, we used specific ubiquitin antibodies (K48 and K63) to detect the type of ubiquitination modification of mitochondrial MFN2 induced by CORT. As shown in Figure 6H, we found that CORT triggers K48-linked ubiquitination of mitochondrial MFN2 instead of K63-linked ubiquitination, which accounts for its proteasomal degradation. These findings collectively support the notion that CORT promotes the proteasomal degradation of mitochondrial MFN2.

The interaction between appoptosin and MFN2 derived by CORT promotes degradation of mitochondrial MFN2, mitochondrial dysfunction, and cardiomyocyte hypertrophy

To elucidate the CORT-induced degradation of mitochondrial MFN2, we conducted a comprehensive analysis utilizing the NCBI protein database and the CELLO subcellular localization predictive system to identify proteins potentially involved in promoting MFN2 ubiquitination modification. Among the proteins interacting with MFN2, appoptosin (encoded by *SLC25A38*) emerged as a promising candidate due to its distinct mitochondrial localization (Figures S6 and S7). Initially, we assessed the impact of CORT on appoptosin expression in H9c2 cells. Remarkably, CORT significantly induced appoptosin expression, with both mRNA and protein levels showing elevation (Figures 7A and 7B). Furthermore, subcellular organelle analysis confirmed the predominant mitochondrial localization of appoptosin rather than the endoplasmic reticulum (Figure 7B). Notably, appoptosin has been reported to interact with MFN2 previously,[38] and our findings revealed that CORT stimulation promoted this interaction (Figure 7C). This suggests that CORT may enhance appoptosin expression, thereby facilitating increased interaction with MFN2.

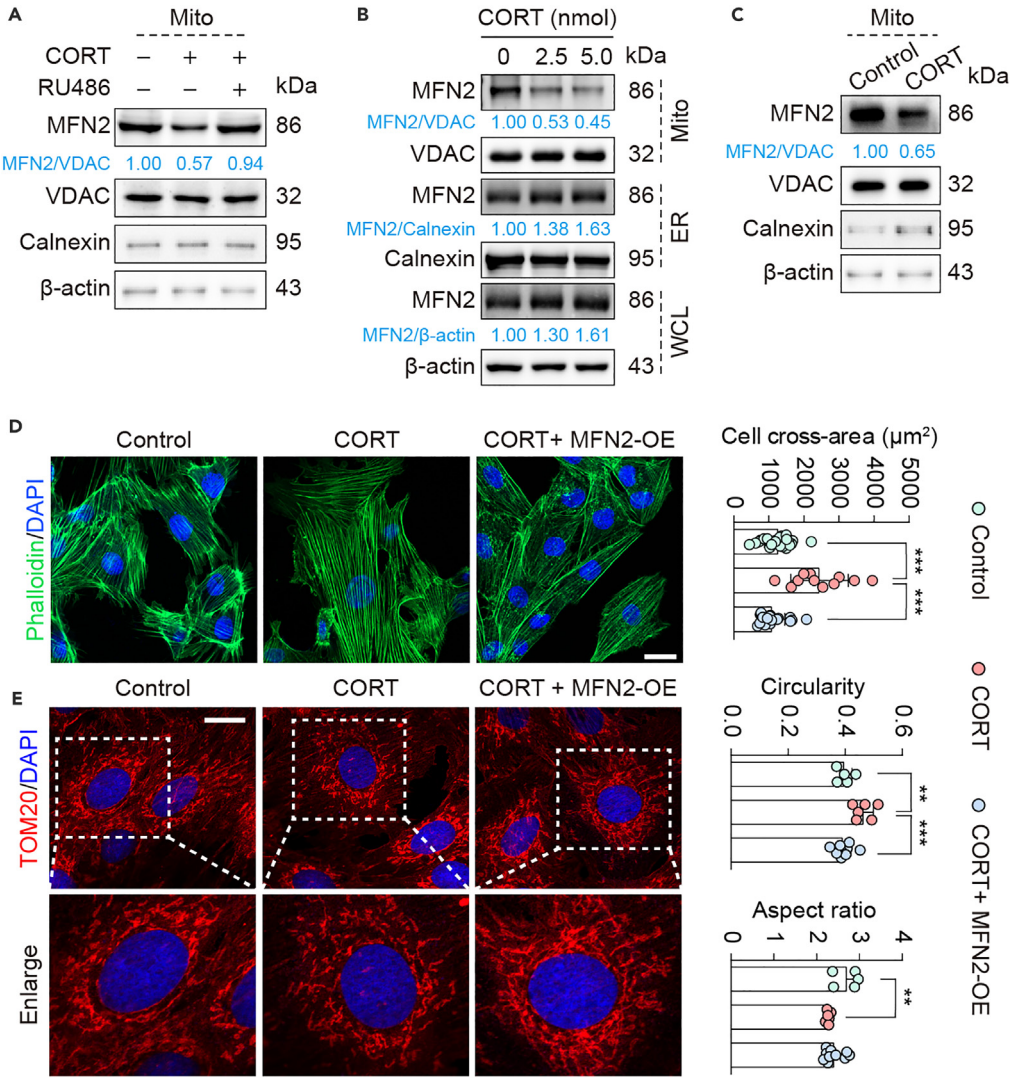

Figure 5. The reduction in mitochondrial MFN2 protein contributes to CORT-induced mitochondrial dysfunction and cardiomyocyte hypertrophy

(A) Western blotting analysis of MFN2 in mitochondria of H9c2 cells. Mito: mitochondria.

(B) Western blotting analysis of MFN2 in mitochondria of hearts from EDD14 chicken embryos. ER, endoplasmic reticulum; WCL, whole-cell lysates.

(C) Western blotting analysis of MFN2 in mitochondria of mice hearts.

(D) Representative confocal images of H9c2 cardiomyocyte stained with phalloidin-FITC. OE, overexpression. Scale bar: 40 μm. The cell cross-area of H9c2 was quantified by ImageJ software.

(E) Mitochondria of H9c2 cells were detected by immunofluorescence with Tom 20 antibody. Scale bar: 40 μm. The mitochondrial area and aspect ratio of H9c2 were analyzed. Data are expressed as the mean ± SD and subjected to statistical analysis using one-way ANOVA followed by Dunnett's multiple comparison test, $^{**}p < 0.01$, $^{***}p < 0.001$ vs. the indicated group.

To further investigate the involvement of appoptosin and its interaction with MFN2 in CORT-induced cardiomegaly, we employed siRNA-mediated silencing of appoptosin in H9c2 cells. The results demonstrated successful inhibition of appoptosin expression by siRNA-2 and siRNA-3, which were subsequently used for further investigations (Figure 7D). As mentioned above, proteasomal degradation of MFN2 within mitochondria contributes to mitochondrial dysfunction and cardiomegaly. Therefore, we evaluated the levels of mitochondrial MFN2 and its ubiquitination upon interference of appoptosin. Of note, *si-appoptosin* ameliorated the CORT-induced reduction in mitochondrial MFN2 levels and attenuated the increase in its ubiquitination (Figures 7E and 7F). In addition, interference of appoptosin also improved CORT-caused impairment of mitochondria. The diminished ATP production was restored to nearly normal levels, and enzyme activities of the respiratory chain complexes showed significant recovery after silence of appoptosin (Figures 7G and 7H). Moreover, interference of appoptosin mitigated the upregulation of four hypertrophy-related genes, including *ANP*, *BNP*, *α-SKA*, and *α-MHC* (Figure 7I). Collectively, these findings suggest that appoptosin may mediate CORT-driven ubiquitination of mitochondrial MFN2, resulting in dysfunction of mitochondria and cardiac hypertrophy.

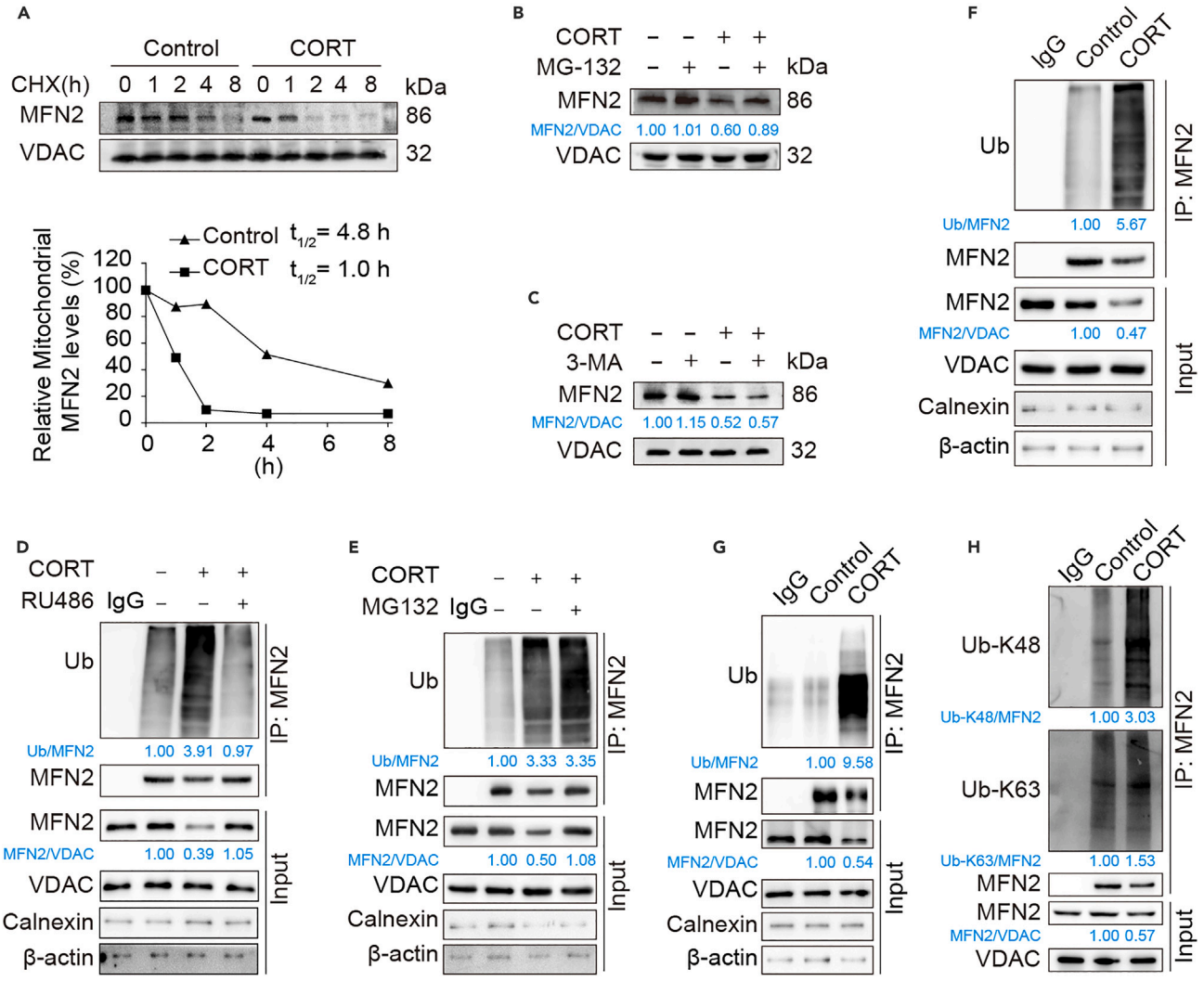

Figure 6. CORT triggers proteasome-dependent degradation of mitochondrial MFN2

(A) Stability of mitochondrial MFN2 was analyzed by western blotting. H9c2 cells were treated with CORT (200 μM) for 48 h followed by CHX (100 μg/mL) over an 8-h time period. Cells were lysed at the indicated time points.

(B and C) Expression of mitochondrial MFN2 in H9c2 cells with CORT (200 μM) and MG-132 (20 μM) or 3-MA (5 mM).

(D) Ubiquitination of mitochondrial MFN2 in H9c2 cells with CORT (200 μM) and RU486 (10 μM).

(E) Ubiquitination of mitochondrial MFN2 in H9c2 cells with CORT (200 μM) and MG-132 (20 μM).

(F and G) Ubiquitination of MFN2 of mitochondria in hearts of chicken embryos and hearts tissue of mice.

(H) Ubiquitination of mitochondrial MFN2 in H9c2 cells detected with Lys48-specific ubiquitin (K48) antibody and Lys63-specific ubiquitin (K63) antibody.

DISCUSSION

Pregnant women are often exposed to external stimuli or experience poor mental states, which can have detrimental effects on fetal heart development. The elevated reactivity of the HPA axis in expectant mothers due to stress represents a potential factor contributing to susceptibility to cardiac hypertrophy in newborns. Herein, we provide evidence that prenatal stress hormone CORT induces cardiac hypertrophy of embryos, which attribute to mechanically fragmentation and dysfunction of mitochondria of cardiomyocyte. Given that mitochondria constitute a significant proportion of cardiomyocyte volume (~30%) and play a crucial role in generating ATP through oxidative phosphorylation to meet the demands of cardiac workload,[39] alterations in mitochondrial structure and function are often associated with pathological changes in the heart. Interestingly, our findings reveal that CORT-induced cardiac hypertrophy is accompanied by mitochondrial fragmentation, suggesting a link between excessive CORT levels and perturbations in mitochondrial morphology. Furthermore, CORT disrupts mitochondrial energy metabolism, resulting in decreased ATP production and impaired activity of respiratory-chain enzymes, which are common features of cardiomyopathy.[40] Previous studies have indicated that mitochondrial dynamics may be involved in the progression of cardiac hypertrophy.[18,41] Du et al. demonstrated that CORT dynamically regulated mitochondrial function by promoting translocation of GR that formed a

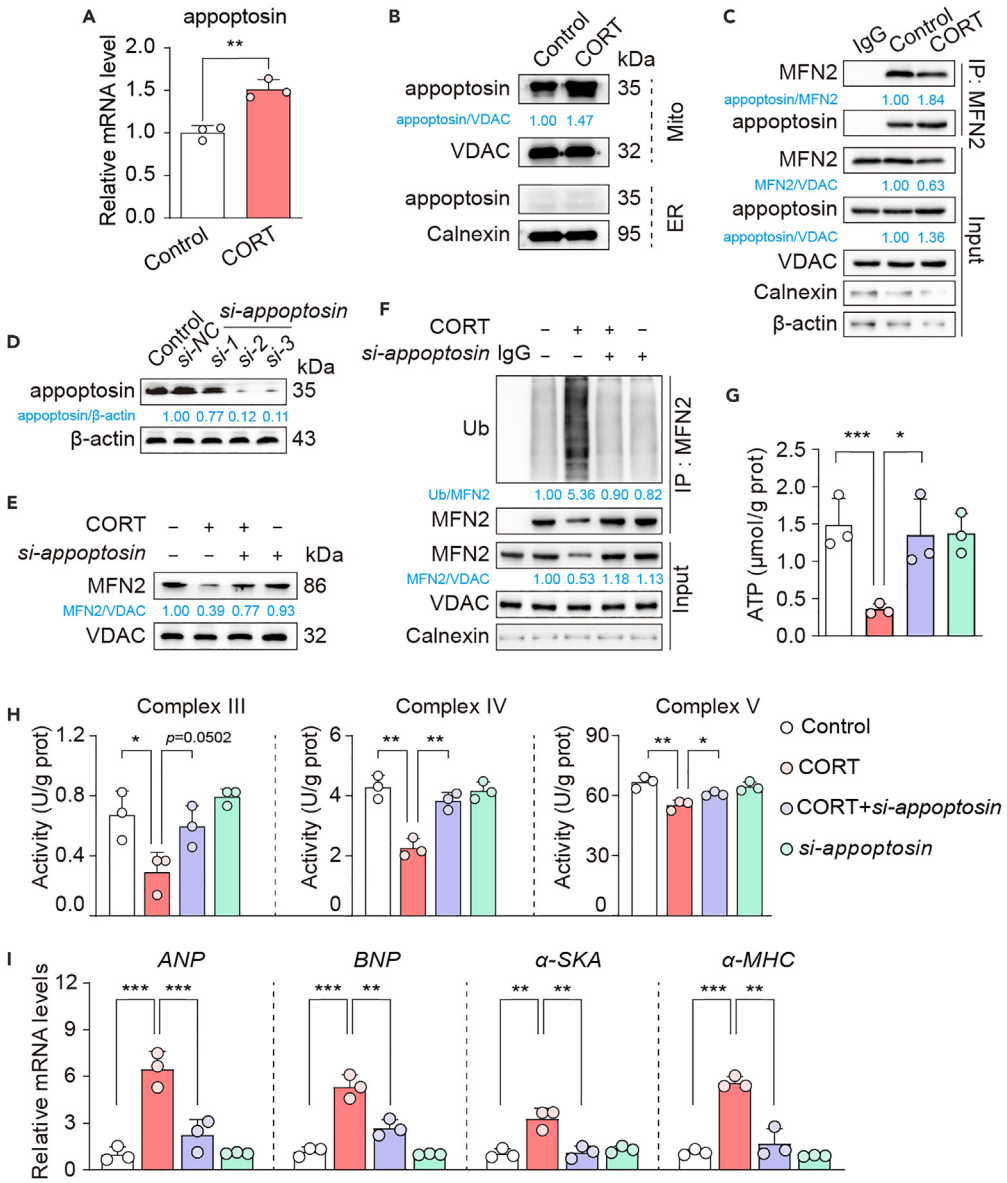

Figure 7. The interaction between appoptosin and MFN2 derived by CORT promotes degradation of mitochondrial MFN2, mitochondrial dysfunction, and cardiomyocyte hypertrophy

(A) The expression of appoptosin mRNA in H9c2 cells detected by qPCR (n = 3).

(B) The level of appoptosin protein detected by western blotting.

(C) The interaction of MFN2 and appoptosin was analyzed by coimmunoprecipitation and western blotting utilizing the corresponding antibodies.

(D) Detection of appoptosin by western blotting in H9c2 cells interfered with *si-appoptosin* for 24 h.

(E) The level of mitochondrial MFN2 in H9c2 with CORT and *si-appoptosin*.

(F) The ubiquitination of mitochondrial MFN2 in H9c2 with CORT and *si-appoptosin*.

(G) The ATP content of H9c2 cells (n = 3).

(H) Enzyme activity of mitochondrial respiratory chain complexes in H9c2 cells (n = 3).

(I) The mRNA levels of four hypertrophy genes, including *ANP*, *BNP*, *α-SKA*, and *α-MHC*, were detected by qPCR in H9c2 cell (n = 3). Data are expressed as the mean ± SD and subjected to statistical analysis using unpaired Student's t test or one-way ANOVA followed by Dunnett's multiple comparison test; *p < 0.05, **p < 0.01, ***p < 0.001 vs. the indicated group.

complex with Bcl-2 into mitochondria.[42] Consistent with these findings, our current study also reveals that myocardial hypertrophy and mitochondrial dysfunction caused by CORT could be reversed by the GR antagonist RU486, suggesting that these pathological changes are dependent on GR activation. Besides, GCs also induce abnormal mitochondrial morphology and dysregulate mitochondrial fusion and fission

in neurons.[43] Additionally, the transcriptional regulation of mitochondrial proteins by GR, acting as a transcription factor, has been previously elucidated.[44] Therefore, prolonged exposure to GCs under stressful conditions may impair mitochondrial quality control in the hearts of offspring.

Mitochondria, as dynamic organelles, undergo a constant cycle of fusion and fission, forming ever-changing tubular networks in most eukaryotic cells. The maintenance of mitochondrial homeostasis relies on the participation of various fusion and fission proteins.[45,46] We discovered that exposure to CORT leads to the degradation of mitochondrial fusion protein MFN2, which contributes to the impairment of mitochondrial network morphology. Zhao et al. demonstrated that knockdown of MFN2 in mouse blastocysts leads to dysfunction of mitochondria and reduces the content of ATP.[47] Considering the distribution of MFN2 in the outer membrane of the mitochondria, mitochondria-associated membranes, and endoplasmic reticulum,[48,49] we isolated organelles and found that CORT decreases the level of MFN2, particularly in mitochondria rather than ER. Intriguingly, in hypertrophic cardiomyocytes induced by phenylephrine or angiotensin II, the expression of MFN2 is also downregulated, and its overexpression promotes mitochondrial fusion and alleviates hypertrophy.[50–53] Indeed, GCs have a angiotensin II-like effect to induce cardiac dysfunction by activating angiotensin II pathway.[54] In addition, the suppressive effect of GCs on MFN2 expression has also been observed in other cells types and tissues.[55–57] Furthermore, we investigated the underlying mechanism by which CORT reduces mitochondrial MFN2 expression from a fresh perspective. We found that CORT promotes the ubiquitination of mitochondrial MFN2 at a post-transcriptional level, leading to its subsequent proteasomal degradation.

Appoptosin (encoded by *SLC25A38*) is a member of the mitochondria carrier family located on the mitochondrial membrane. It plays a crucial role in the transport of glycine and δ-aminolevulinic acid, which are involved in heme biosynthesis.[58] Appoptosin was originally identified as a pro-apoptotic protein associated with neuronal cell death in neurodegeneration.[59,60] Our study presents an innovative perspective that appoptosin mediated CORT-induced cardiac hypertrophy by impairing mitochondrial morphology and function in cardiomyocyte. A previous study verified that appoptosin interacts with mitochondrial outer-membrane fusion proteins, MFN1 and MFN2, and its overexpression could induce mitochondrial fragmentation.[38] In our investigation, we observed an elevated level of appoptosin in response to COTR, which facilitated the recruitment of MFN2 and proteasomal degradation of mitochondrial MFN2. This may underlie the mitochondrial toxicity of appoptosin in cardiac hypertrophy. Although CORT increased the expression of mRNA and protein of appoptosin, it had no impact on appoptosin promoter activity (Figure S8), suggesting that GR may not directly regulate the transcription of appoptosin. Furthermore, appoptosin does not alter the levels of proteins involved in mitochondrial fusion and fission including MFN2.[38] Hence, potential E3 ubiquitin ligases may be recruited to MFN2-appoptosin complex in response to CORT stimulation. We propose that appoptosin may act as a bridging protein, facilitating the recruitment of E3 ubiquitin ligases for the polyubiquitination modification of MFN2. Several E3 ubiquitin ligases have been reported to ubiquitinate MFN2, including Parkin,[61] MARCH5,[62] Mul1,[63] and Huwe1.[64] Among them, Parkin mediates K48 ubiquitination and proteasomal degradation of MFN2. Notably, GCs can promote Parkin expression in the central nervous system through the cAMP response element-binding protein (CREB).[65,66] In addition, in cardiomyocytes, the expression of Parkin also was increased after GCs treatment.[67] Therefore, Parkin may serve as the E3 ligase for the proteasomal degradation of mitochondrial MFN2 in stress-induced cardiac hypertrophy driven by CORT.

Limitations of the study

Although our current study has revealed that prenatal stress hormone CORT triggers embryonic myocardial hypertrophy by inducing ubiquitination and degradation of mitochondrial MFN2 mediated by appoptosin, it is essential to address several limitations. Firstly, stress hormones, including catecholamines and thyroid hormones, in addition to glucocorticoids, should be compared for their effects on embryonic hearts. Furthermore, we did not validate our findings using primary cardiomyocytes *in vitro*. Additionally, the establishment of cell lines and mouse models with appoptosin knockout is crucial to advancing our understanding of the roles played by stress hormones in cardiac hypertrophy. Finally, further exploration of the mechanistic details governing the interaction between MFN2 and appoptosin is warranted. Investigating specific binding domains or critical amino acid residues involved in their interaction would enhance our knowledge of the underlying molecular processes.

STAR★METHODS

Detailed methods are provided in the online version of this paper and include the following:

- KEY RESOURCES TABLE
- RESOURCE AVAILABILITY
  - Lead contact
  - Materials availability
  - Data and code availability
- EXPERIMENTAL MODEL AND STUDY PARTICIPANT DETAILS
  - Animal care
  - Treatment of chicken embryos and mice
  - Cell culture and CORT treatment
- METHOD DETAILS
  - Histological observation

- Echocardiography
- Preparation of subcellular fraction
- Cytoskeleton stained with phalloidin
- Transmission electron microscopy
- RNA isolation and qPCR
- Western blotting
- Detection of MFN2 ubiquitination
- RNA interference and overexpression
- Determination of ATP
- Measurement of respiratory chain enzyme activities
- Mitochondrial morphology detection by confocal microscope
- Seahorse analysis of OXPHOS
- WGA staining

● QUANTIFICATION AND STATISTICAL ANALYSIS

SUPPLEMENTAL INFORMATION

Supplemental information can be found online at https://doi.org/10.1016/j.isci.2023.108690.

ACKNOWLEDGMENTS

This study was partly supported by the National Key Research and Development Program of China (grant number 2017YFC1700404 and 2022YFC0867400), the Natural Science Foundation of China (grant number U1801284, 82125038, 82174054, and 81973718), the Natural Science Foundation of Guangdong (2023B1515040016, 2021A1515011297, and 2021B1515120023), the Local Innovative and Research Teams Project of Guangdong Pearl River Talents Program (grant number 2017BT01Y036), and the Innovation Team Project of Guangdong Provincial Department of Education (2020KCXTD003) and GDUPS (2019). The authors (Rong-Rong He and Yi-Fang Li) also gratefully acknowledge the support of the K.C. Wong Education Foundation.

AUTHOR CONTRIBUTIONS

R-R He and Y-F Li conceptualized and designed the study. C-Y Yan, Y Ye, H-L Mu, T Wu, and W-S Huang performed the experiments and analyzed the data. Y-P Wu, W-Y Sun, S-H Ouyang, and R Wang assisted in experiment. R-R He, Y-F Li, and C-Y Yan wrote the manuscript. L Liang, W-J Duan, X-X Sun, and R-T Huang revised the manuscript. H Kurihara supervised and advised the study. All authors have given approval to the final version of the manuscript.

DECLARATION OF INTERESTS

The authors declare no competing interests.

Received: July 25, 2023
Revised: November 1, 2023
Accepted: December 5, 2023
Published: December 8, 2023

REFERENCES

1. Shimizu, I., and Minamino, T. (2016). Physiological and pathological cardiac hypertrophy. J. Mol. Cell. Cardiol. *97*, 245–262.
2. Samak, M., Fatullayev, J., Sabashnikov, A., Zeriouh, M., Schmack, B., Farag, M., Popov, A.-F., Dohmen, P.M., Choi, Y.-H., Wahlers, T., and Weymann, A. (2016). Cardiac hypertrophy: an introduction to molecular and cellular basis. Med. Sci. Monit Basic Res. *22*, 75–79.
3. Mozaffarian, D., Benjamin, E.J., Go, A.S., Arnett, D.K., Blaha, M.J., Cushman, M., Das, S.R., de Ferranti, S., Després, J.P., Fullerton, H.J., and Howard, V.J. (2016). Heart disease and stroke statistics-2016 update a report from the American Heart Association. Circulation *133*, e38–e360.
4. Heineke, J., and Molkentin, J.D. (2006). Regulation of cardiac hypertrophy by intracellular signalling pathways. Nat. Rev. Mol. Cell Biol. *7*, 589–600.
5. Nakamura, M., and Sadoshima, J. (2018). Mechanisms of physiological and pathological cardiac hypertrophy. Nat. Rev. Cardiol. *15*, 387–407.
6. Louey, S., and Thornburg, K.L. (2005). The prenatal environment and later cardiovascular disease. Early Hum. Dev. *81*, 745–751.
7. Mastorci, F., Vicentini, M., Viltart, O., Manghi, M., Graiani, G., Quaini, F., Meerlo, P., Nalivaiko, E., Maccari, S., and Sgoifo, A. (2009). Long-term effects of prenatal stress: changes in adult cardiovascular regulation and sensitivity to stress. Neurosci. Biobehav. Rev. *33*, 191–203.
8. Graignic-Philippe, R., Dayan, J., Chokron, S., Jacquet, A., and Tordjman, S. (2014). Effects of prenatal stress on fetal and child development: a critical literature review. Neurosci. Biobehav. Rev. *43*, 137–162.
9. Pan, M.-H., Zhu, S.-R., Duan, W.-J., Ma, X.-H., Luo, X., Liu, B., Kurihara, H., Li, Y.-F., Chen, J.-X., and He, R.-R. (2020). "Shanghuo" increases disease susceptibility: Modern significance of an old TCM theory. J. Ethnopharmacol. *250*, 112491.
10. Beijers, R., Buitelaar, J.K., and de Weerth, C. (2014). Mechanisms underlying the effects of prenatal psychosocial stress on child outcomes: beyond the HPA axis. Eur Child Adolesc Psychiatry *23*, 943–956.
11. Werner, J., Sicard, R., Hansen, T., Solomon, E., Cowett, R., and Oh, W. (1992). Hypertrophic cardiomyopathy associated

with dexamethasone therapy for bronchopulmonary dysplasia. J. Pediatr. *120*, 286–291.
12. Israel, B.A., Sherman, F.S., and Guthrie, R.D. (1993). Hypertrophic cardiomyopathy associated with dexamethasone therapy for chronic lung disease in preterm infants. Am. J. Perinatol. *10*, 307–310.
13. Gill, A., Warner, G., and Bull, L. (1996). Iatrogenic neonatal hypertrophic cardiomyopathy. Pediatr. Cardiol. *17*, 335–339.
14. La Mear, N.S., MacGilvray, S.S., and Myers, T.F. (1997). Dexamethasone-induced myocardial hypertrophy in neonatal rats. Biol. Neonate *72*, 175–180.
15. Dodic, M., Samuel, C., Moritz, K., Wintour, E.M., Morgan, J., Grigg, L., and Wong, J. (2001). Impaired cardiac functional reserve and left ventricular hypertrophy in adult sheep after prenatal dexamethasone exposure. Circ. Res. *89*, 623–629.
16. Ohtani, T., Mano, T., Hikoso, S., Sakata, Y., Nishio, M., Takeda, Y., Otsu, K., Miwa, T., Masuyama, T., Hori, M., and Yamamoto, K. (2009). Cardiac steroidogenesis and glucocorticoid in the development of cardiac hypertrophy during the progression to heart failure. J. Hypertens. *27*, 1074–1083.
17. Li, H., Wei, W., and Xu, H. (2022). Drug discovery is an eternal challenge for the biomedical sciences. Acta Mater Med *1*, 1–3.
18. Rosca, M.G., Tandler, B., and Hoppel, C.L. (2013). Mitochondria in cardiac hypertrophy and heart failure. J. Mol. Cell. Cardiol. *55*, 31–41.
19. Ong, S.-B., and Hausenloy, D.J. (2010). Mitochondrial morphology and cardiovascular disease. Cardiovasc. Res. *88*, 16–29.
20. Dorn, G.W., Vega, R.B., and Kelly, D.P. (2015). Mitochondrial biogenesis and dynamics in the developing and diseased heart. Genes Dev. *29*, 1981–1991.
21. Wang, J., and Zhou, H. (2020). Mitochondrial quality control mechanisms as molecular targets in cardiac ischemia–reperfusion injury. Acta Pharm. Sin. B *10*, 1866–1879.
22. Forte, M., Schirone, L., Ameri, P., Basso, C., Catalucci, D., Modica, J., Chimenti, C., Crotti, L., Frati, G., Rubattu, S., et al. (2020). The role of mitochondrial dynamics in cardiovascular diseases. Br. J. Pharmacol. *178*, 2060–2076.
23. Nan, J., Zhu, W., Rahman, M., Liu, M., Li, D., Su, S., Zhang, N., Hu, X., Yu, H., Gupta, M.P., and Wang, J.a. (2017). Molecular regulation of mitochondrial dynamics in cardiac disease. Biochim. Biophys. Acta Mol. Cell Res. *1864*, 1260–1273.
24. Li, A., Gao, M., Jiang, W., Qin, Y., and Gong, G. (2020). Mitochondrial Dynamics in Adult Cardiomyocytes and Heart Diseases. Front. Cell Dev. Biol. *8*, 584800.
25. Wang, Y., Xie, Z., Jiang, N., Wu, Z., Xue, R., Dong, B., Fan, W., Dai, G., Chen, C., Li, J., et al. (2020). Hispidulin attenuates cardiac hypertrophy by improving mitochondrial dysfunction. Front Cardiovasc Med. *7*, 582890.
26. Sotomayor-Flores, C., Rivera-Mejías, P., Vásquez-Trincado, C., López-Crisosto, C., Morales, P.E., Pennanen, C., Polakovicova, I., Aliaga-Tobar, V., García, L., Roa, J.C., et al. (2020). Angiotensin-(1–9) prevents cardiomyocyte hypertrophy by controlling mitochondrial dynamics via miR-129-3p/PKIA pathway. Cell Death Differ. *27*, 2586–2604.
27. Kuzmicic, J., Del Campo, A., López-Crisosto, C., Morales, P.E., Pennanen, C., Bravo-Sagua, R., Hechenleitner, J., Zepeda, R., Castro, P.F., Verdejo, H.E., et al. (2011). Mitochondrial dynamics: a potential new therapeutic target for heart failure. Rev. Esp. Cardiol. *64*, 916–923.
28. Hasan, P., Saotome, M., Ikoma, T., Iguchi, K., Kawasaki, H., Iwashita, T., Hayashi, H., and Maekawa, Y. (2018). Mitochondrial fission protein, dynamin-related protein 1, contributes to the promotion of hypertensive cardiac hypertrophy and fibrosis in Dahl-salt sensitive rats. J. Mol. Cell. Cardiol. *121*, 103–106.
29. Sun, Y.L., Li, S.H., Yang, L., and Wang, Y. (2018). miR-376b-3p attenuates mitochondrial fission and cardiac hypertrophy by targeting mitochondrial fission factor. Clin. Exp. Pharmacol. Physiol. *45*, 779–787.
30. Piquereau, J., Caffin, F., Novotova, M., Prola, A., Garnier, A., Mateo, P., Fortin, D., Huynh, L.H., Nicolas, V., Alavi, M.V., et al. (2012). Down-regulation of OPA1 alters mouse mitochondrial morphology, PTP function, and cardiac adaptation to pressure overload. Cardiovasc. Res. *94*, 408–417.
31. Wang, T., Zhai, M., Xu, S., Ponnusamy, M., Huang, Y., Liu, C.-Y., Wang, M., Shan, C., Shan, P.-P., Gao, X.-Q., et al. (2020). NFATc3-dependent expression of miR-153-3p promotes mitochondrial fragmentation in cardiac hypertrophy by impairing mitofusin-1 expression. Theranostics *10*, 553–566.
32. Papanicolaou, K.N., Khairallah, R.J., Ngoh, G.A., Chikando, A., Luptak, I., O'Shea, K.M., Riley, D.D., Lugus, J.J., Colucci, W.S., Lederer, W.J., et al. (2011). Mitofusin-2 maintains mitochondrial structure and contributes to stress-induced permeability transition in cardiac myocytes. Mol. Cell Biol. *31*, 1309–1328.
33. Hu, L., Ding, M., Tang, D., Gao, E., Li, C., Wang, K., Qi, B., Qiu, J., Zhao, H., Chang, P., et al. (2019). Targeting mitochondrial dynamics by regulating Mfn2 for therapeutic intervention in diabetic cardiomyopathy. Theranostics *9*, 3687–3706.
34. Weber, K.T., Sun, Y., Bhattacharya, S.K., Ahokas, R.A., and Gerling, I.C. (2013). Myofibroblast-mediated mechanisms of pathological remodelling of the heart. Nat. Rev. Cardiol. *10*, 15–26.
35. Watkins, S.J., Borthwick, G.M., and Arthur, H.M. (2011). The H9C2 cell line and primary neonatal cardiomyocyte cells show similar hypertrophic responses in vitro. In Vitro Cell. Dev. Biol. Anim. *47*, 125–131.
36. Pennanen, C., Parra, V., López-Crisosto, C., Morales, P.E., del Campo, A., Gutierrez, T., Rivera-Mejías, P., Kuzmicic, J., Chiong, M., Zorzano, A., et al. (2014). Mitochondrial fission is required for cardiomyocyte hypertrophy mediated by a Ca2+-calcineurin signaling pathway. J. Cell Sci. *127*, 2659–2671.
37. Nathan, J.A., Tae Kim, H., Ting, L., Gygi, S.P., and Goldberg, A.L. (2013). Why do cellular proteins linked to K63-polyubiquitin chains not associate with proteasomes? EMBO J. *32*, 552–565.
38. Zhang, C., Shi, Z., Zhang, L., Zhou, Z., Zheng, X., Liu, G., Bu, G., Fraser, P.E., Xu, H., and Zhang, Y.W. (2016). Appoptosin interacts with mitochondrial outer-membrane fusion proteins and regulates mitochondrial morphology. J. Cell Sci. *129*, 994–1002.
39. Tuomainen, T., and Tavi, P. (2017). The role of cardiac energy metabolism in cardiac hypertrophy and failure. Exp. Cell Res. *360*, 12–18.
40. He, Y., Huang, W., Zhang, C., Chen, L., Xu, R., Li, N., Wang, F., Han, L., Yang, M., and Zhang, D. (2021). Energy metabolism disorders and potential therapeutic drugs in heart failure. Acta Pharm. Sin. B *11*, 1098–1116.
41. Zhou, L.-Y., Liu, J.-P., Wang, K., Gao, J., Ding, S.-L., Jiao, J.-Q., and Li, P.-F. (2013). Mitochondrial function in cardiac hypertrophy. Int. J. Cardiol. *167*, 1118–1125.
42. Du, J., Wang, Y., Hunter, R., Wei, Y., Blumenthal, R., Falke, C., Khairova, R., Zhou, R., Yuan, P., Machado-Vieira, R., et al. (2009). Dynamic regulation of mitochondrial function by glucocorticoids. Proc Natl Acad Sci US A *106*, 3543–3548.
43. Choi, G.E., and Han, H.J. (2021). Glucocorticoid impairs mitochondrial quality control in neurons. Neurobiol. Dis. *152*, 105301.
44. Lapp, H.E., Bartlett, A.A., and Hunter, R.G. (2019). Stress and glucocorticoid receptor regulation of mitochondrial gene expression. J. Mol. Endocrinol. *62*, R121–R128.
45. Bach, D., Pich, S., Soriano, F.X., Vega, N., Baumgartner, B., Oriola, J., Daugaard, J.R., Lloberas, J., Camps, M., Zierath, J.R., et al. (2003). Mitofusin-2 determines mitochondrial network architecture and mitochondrial metabolism A novel regulatory mechanism altered in obesity. J. Biol. Chem. *278*, 17190–17197.
46. Chen, H., Chomyn, A., and Chan, D.C. (2005). Disruption of fusion results in mitochondrial heterogeneity and dysfunction. J. Biol. Chem. *280*, 26185–26192.
47. Zhao, N., Zhang, Y., Liu, Q., and Xiang, W. (2015). Mfn2 affects embryo development via mitochondrial dysfunction and apoptosis. PLoS One *10*, e0125680.
48. Merkwirth, C., and Langer, T. (2008). Mitofusin 2 builds a bridge between ER and mitochondria. Cell *135*, 1165–1167.
49. De Brito, O.M., and Scorrano, L. (2008). Mitofusin 2 tethers endoplasmic reticulum to mitochondria. Nature *456*, 605–610.
50. Zhao, Y., Ponnusamy, M., Liu, C., Tian, J., Dong, Y., Gao, J., Wang, C., Zhang, Y., Zhang, L., Wang, K., and Li, P. (2017). MiR-485-5p modulates mitochondrial fission through targeting mitochondrial anchored protein ligase in cardiac hypertrophy. Biochim. Biophys. Acta, Mol. Basis Dis. *1863*, 2871–2881.
51. Xiong, W., Ma, Z., An, D., Liu, Z., Cai, W., Bai, Y., Zhan, Q., Lai, W., Zeng, Q., Ren, H., and Xu, D. (2019). Mitofusin 2 participates in mitophagy and mitochondrial fusion against angiotensin II-induced cardiomyocyte injury. Front. Physiol. *10*, 411.
52. Yu, H., Guo, Y., Mi, L., Wang, X., Li, L., and Gao, W. (2011). Mitofusin 2 inhibits angiotensin II-induced myocardial hypertrophy. J. Cardiovasc Pharmacol. Ther. *16*, 205–211.
53. Guan, X., Wang, L., Liu, Z., Guo, X., Jiang, Y., Lu, Y., Peng, Y., Liu, T., Yang, B., Shan, H., et al. (2016). miR-106a promotes cardiac hypertrophy by targeting mitofusin 2. J. Mol. Cell. Cardiol. *99*, 207–217.
54. Roy, S.G., De, P., Mukherjee, D., Chander, V., Konar, A., Bandyopadhyay, D., and Bandyopadhyay, A. (2009). Excess of glucocorticoid induces cardiac dysfunction via activating angiotensin II pathway. Cell. Physiol. Biochem. *24*, 1–10.
55. Hernández-Alvarez, M.I., Paz, J.C., Sebastián, D., Munoz, J.P., Liesa, M., Segalés, J., Palacín, M., and Zorzano, A. (2013). Glucocorticoid modulation of mitochondrial function in

hepatoma cells requires the mitochondrial fission protein Drp1. Antioxid Redox Signal *19*, 366–378.

56. Yuan, J., Gao, Y.-s., Liu, D.-l., Tai, A.C.P., Zhou, H., Papadimitriou, J.M., Zhang, C.-q., Zheng, M.-h., and Gao, J.-j. (2023). PINK1-mediated mitophagy contributes to glucocorticoid-induced cathepsin K production in osteocytes. J Orthop Translat. *38*, 229–240.
57. Liu, W., and Zhou, C. (2012). Corticosterone reduces brain mitochondrial function and expression of mitofusin, BDNF in depression-like rodents regardless of exercise preconditioning. Psychoneuroendocrinology *37*, 1057–1070.
58. Guernsey, D.L., Jiang, H., Campagna, D.R., Evans, S.C., Ferguson, M., Kellogg, M.D., Lachance, M., Matsuoka, M., Nightingale, M., Rideout, A., et al. (2009). Mutations in mitochondrial carrier family gene SLC25A38 cause nonsyndromic autosomal recessive congenital sideroblastic anemia. Nat. Genet. *41*, 651–653.
59. Zhang, H., Zhang, Y.-w., Chen, Y., Huang, X., Zhou, F., Wang, W., Xian, B., Zhang, X., Masliah, E., Chen, Q., et al. (2012). Appoptosin is a novel pro-apoptotic protein and mediates cell death in neurodegeneration. J. Neurosci. *32*, 15565–15576.
60. Zhao, Y., Tseng, I.-C., Heyser, C.J., Rockenstein, E., Mante, M., Adame, A., Zheng, Q., Huang, T., Wang, X., and Arslan, P.E. (2015). Appoptosin-mediated caspase cleavage of tau contributes to progressive supranuclear palsy pathogenesis. Neuron *87*, 963–975.
61. McLelland, G.-L., Goiran, T., Yi, W., Dorval, G., Chen, C.X., Lauinger, N.D., Krahn, A.I., Valimehr, S., Rakovic, A., Rouiller, I., et al. (2018). Mfn2 ubiquitination by PINK1/parkin gates the p97-dependent release of ER from mitochondria to drive mitophagy. Elife *7*, e32866.
62. Sugiura, A., Nagashima, S., Tokuyama, T., Amo, T., Matsuki, Y., Ishido, S., Kudo, Y., McBride, H.M., Fukuda, T., Matsushita, N., et al. (2013). MITOL regulates endoplasmic reticulum-mitochondria contacts via Mitofusin2. Mol Cell *51*, 20–34.
63. Yun, J., Puri, R., Yang, H., Lizzio, M.A., Wu, C., Sheng, Z.-H., and Guo, M. (2014). MUL1 acts in parallel to the PINK1/parkin pathway in regulating mitofusin and compensates for loss of PINK1/parkin. Elife *3*, e01958.
64. Leboucher, G.P., Tsai, Y.C., Yang, M., Shaw, K.C., Zhou, M., Veenstra, T.D., Glickman, M.H., and Weissman, A.M. (2012). Stress-induced phosphorylation and proteasomal degradation of mitofusin 2 facilitates mitochondrial fragmentation and apoptosis. Mol. Cell *47*, 547–557.
65. D Pandya, C., Crider, A., and Pillai, A. (2014). Glucocorticoid regulates parkin expression in mouse frontal cortex: implications in schizophrenia. Curr. Neuropharmacol. *12*, 100–107.
66. Ham, S., Lee, Y.-I., Jo, M., Kim, H., Kang, H., Jo, A., Lee, G.H., Mo, Y.J., Park, S.C., Lee, Y.S., et al. (2017). Hydrocortisone-induced parkin prevents dopaminergic cell death via CREB pathway in Parkinson's disease model. Sci. Rep. *7*, 525.
67. Zhou, R., Li, J., Zhang, L., Cheng, Y., Yan, J., Sun, Y., Wang, J., and Jiang, H. (2020). Role of Parkin-mediated mitophagy in glucocorticoid-induced cardiomyocyte maturation. Life Sci. *255*, 117817.

STAR★METHODS

KEY RESOURCES TABLE

REAGENT or RESOURCE	SOURCE	IDENTIFIER
Antibodies		
Rabbit polyclonal anti-Ubiquitin	Abcam	Cat#: ab7780 RRID: AB_306069
Rabbit polyclonal anti-Calnexin	Abcam	Cat#: ab22595 RRID: AB_2069006
Rabbit polyclonal anti-SLC25A38	Abcam	Cat#: ab62224 RRID: AB_943732
Rabbit polyclonal anti-MFN2 (H-68)	Santa Cruz Biotechnology	Cat#: sc-50331 RRID: AB_2142754
Rabbit polyclonal anti-MFN2	Proteintech	Cat#: 12186-1-AP RRID: AB_2266320
Rabbit polyclonal anti-Tom 20	Proteintech	Cat#: 11802-1-AP RRID: AB_2207530
Rabbit monoclonal anti-VDAC (D73D12)	Cell Signaling Technology	Cat#: 4661 RRID: AB_10557420
Mouse monoclonal anti-MHC	DSHB	Cat#: MF20 RRID: AB_2147781
Goat anti-rabbit IgG (Alexa Fluor 555)	Thermo Fisher Scientific	Cat#: Z25305 RRID: AB_2736950
Mouse anti-β-actin	Fude Biological Technology	Cat#: FD0060 RRID: AB_2923199
Mouse anti-GAPDH	Fude Biological Technology	Cat#: FD0063 RRID: AB_2934268
HRP AffiniPure Goat Anti-Rabbit IgG	Fude Biological Technology	Cat#: FDR007 RRID: AB_2934270
HRP AffiniPure Goat Anti-Mouse IgG	Fude Biological Technology	Cat#: FDM007 RRID: AB_2934269
Rabbit monoclonal anti-Lys63 specific ubiquitin	Millipore	Cat#: 05-1308 RRID: AB_1587580
Rabbit monoclonal anti-Lys48 specific ubiquitin	Millipore	Cat#: 05-1307 RRID: AB_1587578
Chemicals, peptides, and recombinant proteins		
CORT	Sigma-Aldrich	Cat#: 802905
RU486	Sigma-Aldrich	Cat#: M8046
Mito Red	Sigma-Aldrich	Cat#: 53271
3-MA	Sigma-Aldrich	Cat#: 189490
L-glutamine	Sigma-Aldrich	Cat#: G5792
Dimethyl sulfoxide (DMSO)	Sigma-Aldrich	Cat#: D8418
Protein A/G PLUS-Agarose	Santa Cruz	Cat#: sc-2003
DAPI	Beyotime Biotechnology	Cat#: C1002
Protease inhibitor cocktail	Beyotime Biotechnology	Cat#: P1005
Cell lysis buffer for Western and IP	Beyotime Biotechnology	Cat#: P0013
5 × SDS-PAGE sample loading buffer	Beyotime Biotechnology	Cat#: P0015B
MG132	Selleck	Cat#: S2619

(*Continued on next page*)

Continued

REAGENT or RESOURCE	SOURCE	IDENTIFIER
WGA Lectin (FITC)	GeneTex	Cat#: GTX01502
Oligomycin	MedChem Express	Cat#: HY-16589
FCCP	MedChem Express	Cat#: HY-100410
Rotenone	MedChem Express	Cat#: HY-B1756
Normal goat serum	Solarbio Life Science	Cat#: SL038
Glucose	Aladdin	Cat#: G116302
Paraformaldehyde	Aladdin	Cat#: C104188
25% glutaraldehyde	Aladdin	Cat#: G359127
PEG 3000	Aladdin	Cat#: P432448
Pyruvate	Gibco	Cat#: 11360070
DMEM	Gibco	Cat#: 11960044
Fetal bovine serum	Gibco	Cat#: 10099141C
Trypsin-EDTA (0.25%)	Gibco	Cat#: 25200072
Triton-100	Sangon Biotech	Cat#: A110694
Non-fat powdered milk	Sangon Biotech	Cat#: A600669
Lipofectamine 2000	Invitrogen	Cat#: 11668019
Lipofectamine 3000	Invitrogen	Cat#: L3000150
Sodium dodecyl sulfate (SDS)	BioFroxx	Cat#: 3250GR500
Albumin Bovine (BSA)	BioFroxx	Cat#: 4240
5 × loading buffer (DTT)	Fude Biological Technology	Cat#: FD002
ECL substrate	Fude Biological Technology	Cat#: FD8020
TRIzol reagent	Invitrogen	Cat#: 15596018
FITC-labeled phalloidin	Yeasen Biotechnology	Cat#: 40735ES75
TRITC-labeled phalloidin	Yeasen Biotechnology	Cat#: 40734ES75
Critical commercial assays		
Mitochondria respiratory chain complex III assay kit	Nanjing Jiancheng Bioengineering Institute	Cat#: A089-3-1
Mitochondria respiratory chain complex IV assay kit	Nanjing Jiancheng Bioengineering Institute	Cat#: A089-4-1
Mitochondria respiratory chain complex V assay kit	Nanjing Jiancheng Bioengineering Institute	Cat#: A089-5-1
ATP assay kit	Nanjing Jiancheng Bioengineering Institute	Cat#: A095-1-1
FastKing RT Kit (With gDNase)	Tiangen Biotech	Cat#: KR116
TransStart® Top Green qPCR SuperMix	TransGen Biotech	Cat#: AQ131-01
Tissue mitochondria isolation kit	Beyotime Biotechnology	Cat#: C3606
Hematoxylin and eosin staining kit	Beyotime Biotechnology	Cat#: C0105
Modified Sirius Red Stain Kit (No Picric Acid)	Solarbio Life Sciences	Cat#: G1472
Pierce BCA Protein Assay Kit	Thermo Fisher Scientific	Cat#: 23225
Experimental models: Cell lines		
H9c2 cells	National Collection of Authenticated Cell Cultures	Cat#: SCSP-5211
Experimental models: Organisms/strains		
Fertilized eggs	South China Agricultural University	N/A
Kunming mice	Guangdong Medical Laboratory Animal Center	https://www.gdmlac.com.cn/
Oligonucleotides		
siRNA targeting sequence #1: appootosin 5′-GTGGGATATTTGCTGGTAT-3′	Guangzhou Rio Bio	N/A
siRNA targeting sequence #2: appootosin 5′-CCACTGAAGTTTCAATGGA-3′	Guangzhou Rio Bio	N/A

(*Continued on next page*)

Continued

REAGENT or RESOURCE	SOURCE	IDENTIFIER
siRNA targeting sequence #3: appootosin 5′-GTCTGTATGTCACCTATCA′	Guangzhou Rio Bio	N/A
Recombinant DNA		
Plasmid: pcDNA3.1-MFN2	This paper	N/A
Plasmid: pcDNA3.1-Vector	This paper	N/A
Software and algorithms		
ImageJ Java 8	ImageJ	https://ImageJ.net/ij/
GraphPad Prism 8.0.2	GraphPad	https://www.graphpad.com/

RESOURCE AVAILABILITY

Lead contact

Further information and requests for resources and reagents should be directed to and will be fulfilled by the lead contact, Rong-Rong He (rongronghe@jnu.edu.cn).

Materials availability

This study did not generate new unique reagents.

Data and code availability

- All data reported in this paper is available within the paper and the supplemental information.
- This paper does not report original code.
- Any additional information required to reanalyze the data reported in this paper is available from the lead contact upon reasonable request.

EXPERIMENTAL MODEL AND STUDY PARTICIPANT DETAILS

Animal care

The Kunming mice were obtained from Guangdong Medical Laboratory Animal Center (Guangzhou, China), and were housed at a temperature of 22°C and a humidity of 55%, under a 12-h light/12-h dark cycle, with access to standard mouse chow diet and water *ad libitum*. Fertilized eggs were purchased from South China Agricultural University (Guangzhou, China), and were incubated at 37°C and 68% humidity in an incubator (Grumbach, Asslar, Germany). All animals were randomly grouped according to the principle of randomization. All animal procedures were conducted in accordance with National Institute of Health's Guide for the Care and Use of Laboratory Animals (7th edition, United States) and were approved by the Institute of Laboratory Animal Center and the Ethics Committee of Jinan university.

Treatment of chicken embryos and mice

On EDD 3, the outline of the air chamber was traced under an illuminator, and a 2 mm hole was punctured at the top of the chamber. Subsequently, CORT (2.5 nmol or 5.0 nmol) was injected into the air chamber, with or without RU486 (5.0 nmol), and this procedure was repeated every other day until EDD 14. Finally, all embryos were harvested for further analysis.

Six-week-old male and female Kunming mice were housed together for mating, and female mice were separated on the second day. After a week, pregnant mice were injected subcutaneously with CORT (2 mg/kg), dissolved in polyethylene glycol 3000 (PEG 3000), once daily until they gave birth to neonatal mice, which took two weeks. The control group received an equal volume of PEG 3000. Hearts from offspring mice (newborn or four-week-old) were collected for further analysis after anesthesia with isoflurane.

Cell culture and CORT treatment

H9c2 cardiomyocytes from passage 5–10 were cultured in Dulbecco's modified Eagle's medium (DMEM) supplemented with 10% fetal bovine serum (FBS) at 37°C in a 5% CO2 incubator. The H9c2 cardiomyocytes were treated with 200 μM CORT for 48 h to induce cellular hypertrophy. To antagonize the GR, RU486 was added to H9c2 cells simultaneously with CORT.

METHOD DETAILS

Histological observation

The hearts were harvested from chicken embryos and mice and fixed in 4% paraformaldehyde (PFA), and were subsequently dehydrated, embedded in paraffin, and sectioned at a thickness of 5 μm. The sections were then dewaxed in xylene and rehydrated using an ethanol

gradient. Hematoxylin eosin (H&E) staining was performed according to the instructions provided in the staining kit (C0105, Beyotime Biotechnology). Briefly, the sections were soaked in hematoxylin solution for 5 min and washed with flowing water for 5 min. Eosin staining was then performed for 3 min, followed by a 2-min washing with flowing water. For the assessment of myocardial tissue fibrosis, the Sirius Red staining experiment was conducted using a commercial kit. Finally, all sections were dehydrated and vitrified using conventional protocols. The histological morphology of the sections was observed and photographed using an automated scanning microscope.

Echocardiography

Fertilized eggs were exposed to CORT as described until EDD 14. Transthoracic echocardiographic examinations were carried out using the Vevo770 imaging system (Visual Sonics Inc., Toronto, Ontario, Canada).

Preparation of subcellular fraction

Mitochondria and cytosol were fractionated using a cell mitochondria isolation kit (C3606, Beyotime Biotechnology, Shanghai, China) following the manufacturer's protocol. Freshly harvested hearts were rinsed with PBS, minced into small pieces, and treated with trypsin on ice for 20 min, followed by centrifugation at 800 rpm for 5 min to pellet the tissue. Meanwhile, cells were centrifuged at 800 rpm for 5 min at 4°C. The resulting samples were suspended in mitochondria isolation solution containing a protease inhibitor cocktail and homogenized on ice using a tight-fitting pestle attached to a homogenizer. The homogenate was then centrifuged at varying speeds to separate the mitochondria and cytosol fractions.

Cytoskeleton stained with phalloidin

To determine the cytoskeleton, phalloidin staining was performed. The cells were washed three times with PBS and fixed with 4% PFA for 10 min at room temperature. They were then permeabilized with 0.5% Triton X-100 for 5 min and stained with 100 nM FITC-labeled or TRITC-labeled phalloidin (40735ES75/40734ES75, Yeasen Bio Technologies, Shanghai, China) for 30 min at room temperature. The nucleus was stained with 5 μg/mL DAPI (C1002, Beyotime Biotechnology, Shanghai, China). Confocal images were acquired using a Zeiss LSM800 microscope (Jena, Germany).

Transmission electron microscopy

In brief, H9c2 cells or fresh heart tissues were fixed in 2.5% glutaraldehyde overnight at 4°C for 30 min. Specimens were rinsed in PBS, and postfixed in 1% osmium tetroxide at 4°C for 1 h. After dehydrated in acetone; cells were embedded in EPON812. Ultra-thin sections (50–70 nm) from longitudinal parts were cut and examined in a transmission electron microscope (Tecnai 10, FEI) at 80 kV.

RNA isolation and qPCR

Total RNA was isolated using the TRIzol reagent (Invitrogen, 15596018). The concentration of RNA was determined from spectrophotometric analysis at A260/280. First-strand cDNA was synthesized using FastKing RT Kit (TIANGEN, Beijing, China) at 42°C for 15 min. Polymerase chain reaction (PCR) amplification of the cDNA was performed using SYBR qPCR Master Mix (AQ211-01, TransGen Biotech, Beijing, China) on real-time PCR detection system (Bio-Rad, Hercules, CA, USA). 18S was used as an internal control.

Western blotting

Protein samples were separated by SDS-PAGE gels and transferred onto PVDF membranes with a pore size of 0.45 μm. The membranes were blocked with 5% non-fat milk in TBST at room temperature for 1 h. After being blocked, the membranes were incubated with primary antibodies overnight at 4°C. The following day, the membranes were washed with TBST and incubated with secondary antibodies conjugated with horseradish peroxidase (HRP) for 2 h at room temperature. Finally, the membranes were visualized using an ECL substrate (FD8020, Fude Biological Technology) and imaged with a luminescent image analysis system (Tanon 5200, Shanghai, China).

Detection of MFN2 ubiquitination

Cells or heart tissues were lysed using a lysis buffer containing with 0.1% SDS and protease inhibitor cocktail. After centrifugation at 12000 rpm for 10 min at 4°C, the supernatant, containing 500 μg of protein, was subjected to immunoprecipitation. The supernatant was incubated with anti-MFN2 antibody (1 μg) overnight at 4°C, followed by incubation with 30 μL of protein A/G plus agarose for 2.5 h at 4°C. The immunoprecipitate was washed three times with lysis buffer and then boiled in 2 × SDS loading buffer for 5 min. The obtained samples were separated by SDS-PAGE and MFN2 ubiquitination was detected with anti-Ubiquitin antibody.

RNA interference and overexpression

Small interfering RNA (siRNA) technology was used to knock down appoptosin. The target DNA sequences of three siRNAs are 5′-GTGGGA TATTTGCTGGTAT-3′; 5′-CCACTGAAGTTTCAATGGA-3′; 5′-GTCTGTATGTCACCTATCA′. A non-targeting siRNA served as the negative control. All sequences were synthesized by Rio Bio Co., Ltd. (Guangzhou, China). H9c2 cells were transfected with 50 nM *si-appoptosin* using

Lipofectamine 2000 (Invitrogen, CA, USA). For the overexpression of MFN2 *in vitro*, the plasmid pcDNA3.1-MFN2 was transfected to H9c2 cells using Lipofectamine 3000 reagent. After 24 h of transfection, cells were treated with CORT for an additional 48 h.

Determination of ATP

Fresh embryonic hearts were homogenized by a homogenizer in 4% perchloric acid and then centrifuged at 12000 rpm for 10 min. Add 1 M K_2HPO_4 into supernatant followed by another centrifugation at 12000 rpm for 10 min. The resulting supernatant was filtered by 0.22 μm membrane for high-performance liquid chromatography (HPLC) analysis. Detection conditions: UV detection wavelength: 254 nm; column: 5 μm Cosmosil C18 reversed-phase column (250 mm × 4.6 mm, i. d.); sample size: 20 μL; column temperature: room temperature; mobile phase: 50 mM potassium dihydrogen phosphate buffers (pH 6.5); flow rate: 1 mL/min. The ATP peak of samples was determined in reference to the ATP standards. The amount of ATP in samples was determined based on the regression equation from ATP standard. For the evaluation of ATP content of H9c2 cells, a commercial kit was used according to manufacturer's instructions (A095-1-1, Nanjing Jiancheng Bioengineering Institute, Nanjing, China). ATP levels were normalized to protein content.

Measurement of respiratory chain enzyme activities

Mitochondria samples from embryonic hearts or H9c2 cells were used to detect the activities of respiratory chain enzymes (complex III, IV, and V) according to the instructions provided by the kits (A089-3-1, A089-4-1, A089-5-1, Nanjing Jiancheng Bioengineering Institute, Nanjing, China). The enzyme activities of all samples were normalized to protein content determined by BCA kit.

Mitochondrial morphology detection by confocal microscope

H9c2 cells were fixed in 4% PFA for 10 min, permeabilized by 0.2% Triton-100 for 10 min, and blocked with 5% BSA for 1 h at room temperature. Next, cells were incubated with anti-Tom 20 (1:100, Rabbit) at 4°C overnight, followed by incubation with a rabbit secondary antibody conjugated with Alexa Flour 555 (1:500) at room temperature for 2 h. In Mito-Red experiment, H9c2 cells was directly incubated with Mito-Red (100 nM) at 37°C for 45 min. Finally, cells were stained with DAPI (5 μg/mL) for 10 min. Images were obtained on a confocal microscope (Zeiss LSM80, Jena, Germany).

Seahorse analysis of OXPHOS

After being treated with 200 μM CORT for 48 h, H9c2 cells were incubated with freshly prepared medium containing 10 mM glucose, 1 mM pyruvate and 2 mM L-glutamine. Simultaneously, 1 μM oligomycin, 1.5 μM FCCP, and 1 μM antimycin A and 1 μM rotenone were added according to the general experimental procedure. Calibration and measurement were then executed with the Seahorse XFe24 Analyzer. Mitochondrial fractions from the mouse hearts were isolated for the detection of OCR using the same method.

WGA staining

Five-microns sections were deparaffinized and rehydrated following standard procedures. Antigen retrieval was achieved by boiling sections in citric acid buffer (pH 6.0) for 15 min. To block non-specific protein binding, sections were incubated with 5% goat serum for 1 h at room temperature. Next, sections were incubated with FITC-labeled WGA (1: 500) overnight at 4°C. Finally, DAPI was applied to label the nucleus. Fluorescence detection and imaging were conducted using a confocal microscopy.

QUANTIFICATION AND STATISTICAL ANALYSIS

Statistical analyses were carried out using Prism 8 (GraphPad Software, La Jolla, CA, USA). All values were compared by unpaired, two-tailed Student's *t*-test between two groups or one-way analysis of variance (ANOVA) followed by post hoc comparisons with Dunnett's test between multiple groups. $p < 0.05$ was considered statistically significant.